J Infrared Milli Terahz Waves (2016) 37:1124–1138
DOI 10.1007/s10762-016-0308-3

Millimeter Waveband Dielectric Properties of Nanocomposite Materials Based on Opal Matrices with Particles of Spinels

A. B. Rinkevich[1] · **D. V. Perov**[1] · **Ya A. Pakhomov**[1] · **M. I. Samoylovich**[2] · **E. A. Kuznetsov**[3]

Received: 1 June 2016 / Accepted: 25 August 2016 /
Published online: 3 September 2016

Abstract The dielectric properties of 3D nanocomposites based on opal matrices containing the particles of compounds with spinel structure have been studied. Microwave measurements have been carried out in the frequency range from 26 to 38 GHz. The frequency dependences of transmission and reflection coefficients are obtained. The values of the real and imaginary parts of complex dielectric permittivity have been retrieved. The X-ray phase analysis of the nanocomposites is performed and their structures are studied.

Keywords Opal matrix · Spinel, nanocomposite · Microwave measurement · High-frequency complex permittivity · Effective permittivity of nanocomposite material

1 Introduction

Opal matrix is a promising material used in photonics [1]. Completely new modification of opal matrices to create tunable microwave devices is in filling between the spherical voids with

✉ D. V. Perov
peroff@imp.uran.ru

A. B. Rinkevich
rin@imp.uran.ru

M. I. Samoylovich
samoylovich@technomash.ru

[1] M.N. Miheev Institute of Metal Physics, Ural Branch of RAS, 18 S. Kovalevskaya St, Ekaterinburg 620990, Russia

[2] Central Research Technological Institute "TECHNOMASH", 4 I. Franko St, Moscow 121108, Russia

[3] Nizhny Tagil branch of the Ekaterinburg State Social-Pedagogical University, 57 Krasnogvardeyskaya St, Nizhny Tagil 622031, Russia

magnetic materials. In this case, the description of phenomena in the nanocomposites of this kind is possible on the basis of the concept of the ensemble of microspheres and matrices as magnonic and photonic crystals [2, 3]. The opal matrix is useful to create a medium with negative refractive index. Physical properties and structure of opal matrices filled with metallic or ferromagnetic nanoparticles have been studied more thoroughly in [4]. Ferrites with the spinel structure seem to be appropriate materials for such filling because of the combination of properties such as high magnetization, narrow hysteresis loop, and therefore small magnetic losses, high electrical resistivity and small dielectric loss, high Curie temperature, and chemical stability. In the works in [5, 6], the magnetic and microwave properties of 3D nanocomposites based on opal matrix with the particles of nickel-zinc ferrite have been studied; and the magnetic antiresonance phenomenon has been first discovered in the nanocomposite material. Dielectric properties of the 3D nanocomposite materials with particles of the titanates have been investigated in [7]. The aim of present work is a detailed study of the dielectric properties of 3D nanocomposites with particles of several groups of substances with the structure of spinel. The relation between the frequency dependences of measured transmission and reflection coefficients and the complex permittivity has been determined.

2 Structure and Phase Composition of Nanocomposite Materials Based on Opal Matrices

2.1 Synthesis

The synthesis of samples of opal matrices with the diameter of SiO_2 spheres from 200 to 350 nm has been described in several papers; see, e.g., [4, 8]. Nanocomposites with embedded nanoparticles of materials with spinel structure are obtained by impregnation with subsequent heat treatment. The properties of nanocomposite materials depend largely on the production technology. The synthesis of samples of opal matrices is performed using the following technology. At the initial stage, branched nanoparticles of amorphous SiO_2 are obtained by the reaction of hydrolysis tetraethyl orthosilicate acid $Si(OC_2H_5)_4$ with a solution of ethanol C_2H_5OH in the presence of a catalyst of ammonium hydroxide NH_4OH. Then, in the process of polycondensation, they turn into the spherical particles of amorphous silicon dioxide. After settling of the precipitate, suspension becomes a hydrogel with the liquid content up to 50–60 wt.%. If the additional precautions are not undertaken, the chalk-like flimsy material will be obtained after drying. Therefore, the heat treatment has been carried out to harden the obtained opal matrices and remove free moisture. The structure of opal matrix is a densely packed periodic structure of submicron spheres. This is indicated by the results of X-ray phase analysis and electron microscopy. The control of correctness of packing nanospheres is performed by analyzing of the shape and width of the bands of the Bragg reflection.

The impregnation method is one of the easiest ways of introduction of various chemical elements and compounds in opal matrix. It is based on the impregnation of the opal matrix substance precursor with a specific chemical composition and involves a subsequent heat treatment, which provides forming of the necessary chemical composition inside the interspherical voids inside the opal matrix. To obtain the embedded particles, the precursors have to be well soluble in water and transformable into the oxides at moderate temperatures of heat treatment; they have not to violate the packing structure of the opal spheres. In this work, the soluble nitrates of metals are used as precursors. During the impregnation procedure, which

is repeated many (up to 10) times, the interspherical space of opal matrix is gradually being filled. After deposition, the substances of the introduced particles are oxides of metals.

The subsequent heat treatment is carried out over a temperature range from 500 to 1100 °C. Under the process of heat treatment, partial thermal decomposition of nitrogroups happens; and residual water is removed completely. After the introduction of the particles, a large part of the substance is concentrated in the space between the spheres. Nanoparticles of substances with the structure of spinel are formed from the oxides of metals.

In this work, the following system of sample designation is adopted. For example, the name No. 175/2-840 means that this sample has a serial number 175, 2 repetitions of the impregnation procedure have been fulfilled, and the temperature of final heat treatment is equal to 840 °C.

2.2 Electron Scanning Microscopy

The structure of nanocomposites has been investigated with the use of the scanning electron microscope Quanta-200. Figure 1 shows the structure of nanocomposites with particles of Ni-Zn ferrite with magnification of ×100,000 and an accelerating voltage of 30 kV. The introduced particles are of irregular shape and they are sized from 10 to 60 nm.

2.3 X-ray Diffraction Analysis

The X-ray phase analysis was carried out using diffractometers DRON-3M and DRON-6 with CuKα radiation. The flat graphite monochromator has been used, and rotation of a sample has been fulfilled in the step mode with a step size of 0.02° as well as in the continuous mode with the angular speed of 1°/min.

As an example, we consider the results of the X-ray diffraction analysis of sample No. 175/2-840—the opal matrix with compounds based on Ni, Zn, and Fe synthesized in nanovoids.

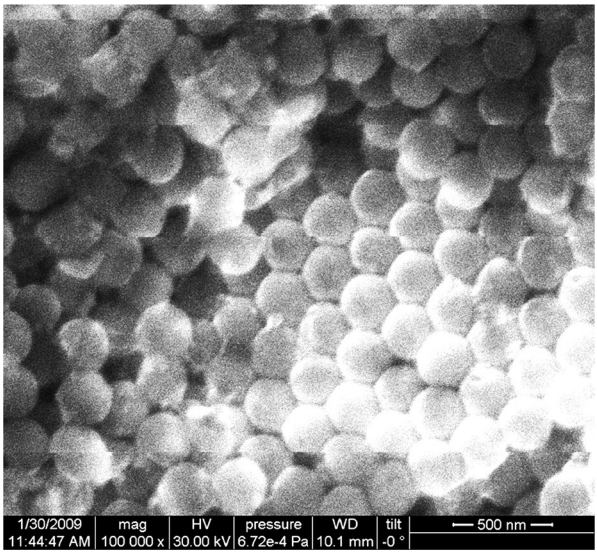

Fig. 1 Structure of the nanocomposites based on opal matrix with the particles of Ni-Zn ferrite, which is observed using the scanning electron microscope, magnification of ×100,000

The analysis allows us to determine the next phase: $Ni_{1-x}Zn_xFe_2O_4$ (structural type of the magnetite–spinel) cubic system, space group Fd3m (85–1436).

As another example, we consider the results of X-ray diffraction analysis of sample No. 190/3-900—the opal matrix with compounds based on Co synthesized in nanovoids. The analysis allows us to determine the next phase: $CoCo_2O_4$ cubic system, space group Fd3m (80–1544). The X-ray diffraction pattern of the sample is presented in Fig. 2, and the X-ray data are summarized in Table 1.

The X-ray diffraction analysis of sample No. 4/5-1100, the opal matrix with compounds based on Mn, Zn, and Fe synthesized in nanovoids, allows to establish the next phase: Mn-Zn-Fe spinel Mn1-xZnxFe2O4, structure type Fe3O4 (magnetite) is a cubic system, space group Fd3m (85–1436).

3 Microwave Measurements of the Transmission and Reflection Coefficients

3.1 Theoretical Basis

Microwave measurements have been performed over a frequency range from 26 to 38 GHz using a standard rectangular waveguide working in the single-mode regime with the use of TE_{10} mode. The measurement technique is like that has been used in [7, 9]. To perform a microwave measurement, a sample is placed across the waveguide as it is shown in Fig. 3. The sample size is 7.2 × 3.6 mm. Microwave experiments have been performed at room temperature using scalar network analyzer. The frequency dependences of the absolute values of transmission T and reflection R coefficients have been measured to evaluate the complex permittivity $\varepsilon \cdot = \varepsilon' - i\varepsilon''$.

Let us consider the interaction of electromagnetic wave with a dielectric sample placed across the rectangular waveguide. The lengths of the inner sides of the waveguide are a and b, where a corresponds to the longest side of the waveguide. The thickness of the sample, i.e., its size along the waveguide axis, is equal to d.

We have used the specimens with the thickness of 2 mm, which fill up completely the cross section of the waveguide, as shown in Fig. 3. We assume that the volume of the waveguide can

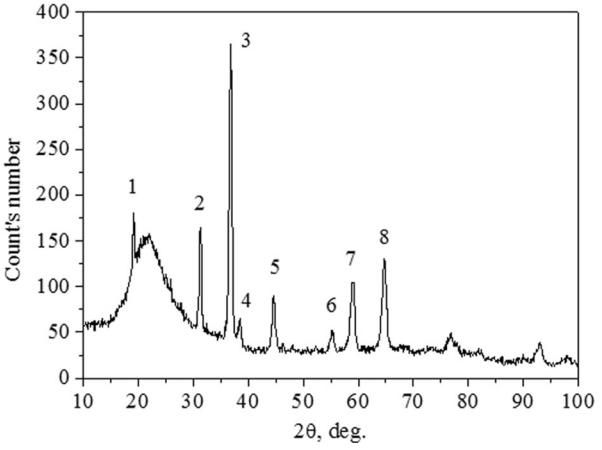

Fig. 2 The result of X-ray phase analysis of sample No. 190/3-900 with $CoCo_2O_4$ nanoparticles

Table 1 The X-ray data for sample No. 190/3-900

Peak's number in Fig. 1	Experimental data				Data ICDD PDF-2 on $CoCo_2O_4$		
	Intensity, %	Bragg angle 2θ, deg.	Half-width of a peak, deg.	Interplanar spacing d, Å	$CoCo_2O_4$ cubic system, sp. group Fd3m (80–1544)		
					d, Å	hkl	I, %
1	11.16	18.98	0.30	4.670	4.708	111	15.6
2	27.44	31.17	0.40	2.866	2.883	220	31.5
3	100.00	36.66	0.51	2.449	2.458	311	100
4	7.91	38.33	0.51	2.346	2.354	222	9.5
5	23.72	44.52	0.61	2.033	2.038	400	19.9
6	10.70	55.13	0.78	1.664	1.664	422	7.8
7	38.14	58.86	0.78	1.567	1.569	511	27.8
8	48.37	64.63	0.78	1.440	1.441	440	32.2

be divided, conventionally, into three regions: regions 1 and 3 are free spaces inside the waveguide situated, respectively, before and after the sample, which is region 2, in the direction of the wave propagation. It is obvious that regions 1 and 3 have the same impedance; we can designate it as Z_1 and the impedance of region 2 as Z_2. It is evident that $Z_1 = \sqrt{\frac{\mu_0}{\varepsilon_0}}$, where μ_0 and ε_0 are the magnetic and electric constants, respectively.

The complex wave number k is determined generally by the formula

$$k = k' - ik'' = \frac{\omega}{c}\sqrt{\varepsilon\mu}, \tag{1}$$

where $\varepsilon = \varepsilon' - i\varepsilon''$ is the complex permittivity, $\mu = \mu' - i\mu''$ is the complex permeability, c is the electromagnetic wave speed in vacuum, and ω is the circular frequency. Components of the wave numbers k are given by the following relations:

$$k' = \sqrt{\frac{1}{2}\left(\sqrt{\Re^4 + \Im^4} + \Re^2\right)}, k'' = \sqrt{\frac{1}{2}\left(\sqrt{\Re^4 + \Im^4} - \Re^2\right)}, \tag{2}$$

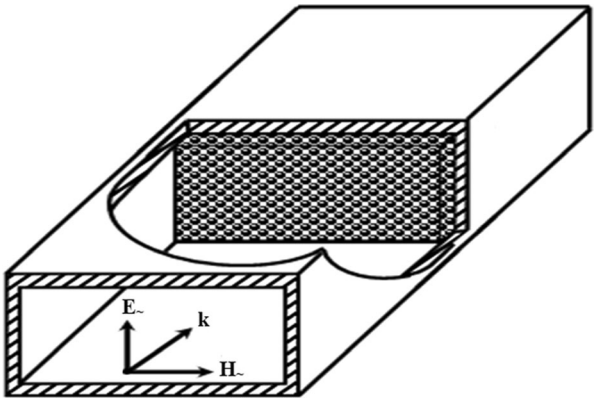

Fig. 3 The sample location in the waveguide for microwave measurements

where

$$\mathfrak{R} = \sqrt{\left(\frac{\omega}{c}\right)^2 (\varepsilon' \mu' - \varepsilon'' \mu'') - \chi_{10}^2}, \quad \mathfrak{I} = \frac{\omega}{c} \sqrt{(\varepsilon'' \mu' + \varepsilon' \mu'')}. \tag{3}$$

In formula (3), χ_{10} is the transverse wave number for TE_{10} mode: $\chi_{10} = \frac{\pi}{a}$.

We believe that region 2 of the waveguide is filled with a non-magnetic imperfect dielectric, so $\varepsilon' = \varepsilon$, $\varepsilon'' = \frac{\sigma}{\omega \varepsilon_0}$, $\mu' = 1$, $\mu'' = 0$. Hence, formula (3) for region 2 can be rewritten in the following form:

$$\mathfrak{R}_2 = \sqrt{\left(\frac{\omega}{c}\right)^2 \varepsilon - \left(\frac{\pi}{a}\right)^2}, \quad \mathfrak{I}_2 = \frac{\omega}{c} \sqrt{\varepsilon''} \tag{4}$$

From expressions (2), (3), and (4), we get that

$$k_2 = k_2' - i k_2'' = \sqrt{\frac{1}{2}\left(\sqrt{\mathfrak{R}_2^4 + \mathfrak{I}_2^4} + \mathfrak{R}_2^2\right)} - i \sqrt{\frac{1}{2}\left(\sqrt{\mathfrak{R}_2^4 + \mathfrak{I}_2^4} - \mathfrak{R}_2^2\right)} \tag{5}$$

The characteristic impedance of region 2, filled with dielectric, can be expressed as

$$Z_2 = \frac{\omega \mu_0}{k_2} = \frac{\omega \mu_0}{k_2' - i k_2''} \tag{6}$$

Complex coefficients of transmission T and reflection R for the waveguide with the sample placed inside is expressed by the following formulas [6]:

$$T = \frac{1}{\cos k_2 d + \frac{1}{2} i \left(\xi + \frac{1}{\xi}\right) \sin k_2 d} \tag{7}$$

and

$$R = \frac{\frac{1}{2} i \left(\xi - \frac{1}{\xi}\right) \sin k_2 d}{\cos k_2 d + \frac{1}{2} i \left(\xi + \frac{1}{\xi}\right) \sin k_2 d}, \tag{8}$$

where $\xi = Z_2 / Z_1$.

Now we briefly examine the procedure for restoring the complex dielectric permittivity of the sample from the transmission and reflection frequency spectra [10]. We denote the experimentally measured moduli of the transmission and reflection coefficients as $|T = T^*(\omega, \varepsilon', \varepsilon'')|$ and $|R = R^*(\omega, \varepsilon', \varepsilon'')|$, respectively. In general, the coefficients are frequency-dependent quantities depending on unknown complex permittivity $\varepsilon = \varepsilon' - i\varepsilon''$.

We write the differences between the moduli of the experimental and calculated transmission coefficients $\Delta_T(\omega, \varepsilon', \varepsilon'') = |T(\omega, \varepsilon', \varepsilon'')| - |T^*(\omega, \varepsilon', \varepsilon'')|$ and appropriate reflection coefficients $\Delta_R(\omega, \varepsilon', \varepsilon'') = |R(\omega, \varepsilon', \varepsilon'')| - |R^*(\omega, \varepsilon', \varepsilon'')|$. To find the unknown permittivity $\varepsilon = \varepsilon' - i\varepsilon''$, the least squares method is used to minimize the value $(\Delta(\varepsilon'^*, \varepsilon''^*))^2$:

$$\left(\Delta\left(\varepsilon'^*, \varepsilon''^*\right)\right)^2 = \min_{\varepsilon' = \varepsilon'^*} \min_{\varepsilon'' = \varepsilon''^*} \left[\left(\Delta_R\left(\omega, \varepsilon', \varepsilon''\right)\right)^2 + \left(\Delta_T\left(\omega, \varepsilon', \varepsilon''\right)\right)^2\right]. \tag{9}$$

Here the values ε'^* and ε''^* are the estimations of real and imaginary part of complex permittivity averaged over a frequency range from 26 to 38 GHz.

3.2 Ferrite Spinels

The measuring results of the frequency dependences of transmission and reflection coefficients for the nanocomposites containing particles of ferrite spinels are presented below. Figure 4 shows the frequency dependence of transmission and reflection coefficients and dissipation of microwave power for a nanocomposite containing particles of cobalt-zinc ferrite: $Co_{0.35}Zn_{0.65}Fe_2O_4$. This ferrite is often used in radiofrequency devices up to tens of megahertz as ferrite core of transformers, antennas, and other devices [11]. This ferrite has the highest saturation magnetization in the system $Co_xZn_{1-x}Fe_2O_4$. The use of bulk samples of ferrite spinels is limited to frequencies in units of gigahertz, in any case, not higher than 10 GHz. In the present work, we study the samples of nanocomposites containing nanoparticles of several compounds with the spinel structure, because preliminary studies have shown that nano-spinels have better frequency characteristics in comparison with bulk ones.

For the nanocomposites with particles of cobalt-zinc ferrite in Fig. 4, one can see the following tendencies: with increasing frequency, the transmission coefficient increases and reflection coefficient decreases. The frequency dependences of the coefficients are determined by several important factors: the frequency dependence of complex permeability, the dispersion of TE_{10} mode in the waveguide, and the proximity of the considered frequency range to the resonant frequencies, when the thickness of a specimen is equal to an integer number of quarter and half wavelength.

Figure 4 shows also the frequency dependence of electromagnetic power dissipation that can be obtained using the relation $1-|T|^2-|R|^2$. This value shows the part of power loss in the sample. As can be seen from Fig. 4, the electromagnetic power dissipation in this material in general increases with increasing frequency. All dependences in Fig. 4 have small-scale oscillations associated with incomplete matching of the microwave circuit. From the data shown in Fig. 4, it can be concluded that for the sample with particles of spinel $Co_{0.35}Zn_{0.65}Fe_2O_4$ the transmission coefficient reaches the largest value in the range 32–38 GHz.

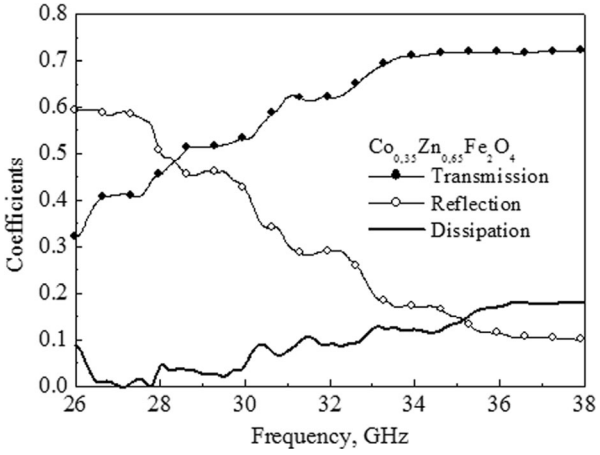

Fig. 4 The frequency dependences of transmission and reflection coefficients and dissipation for the nanocomposites containing particles of cobalt-zinc ferrite $Co_{0.35}Zn_{0.65}Fe_2O_4$

Now we examine the frequency dependences of transmission and reflection coefficients, and dissipation power, for nanocomposites containing particles of nickel-zinc ferrite $Ni_{0.5}Zn_{0.5}Fe_2O_4$. These dependences are shown in Fig. 5a. For the transmission and reflection coefficients, we see the same trends as for the nanocomposites with particles of cobalt-zinc ferrite: with increasing frequency, the transmission coefficient increases and reflection coefficient decreases. The magnitude of the reflection coefficient in the range of 32–38 GHz is very small, ~0.1, that may find practical application. The amount of dissipated electromagnetic power for the sample with nickel-zinc ferrite is much larger than for the samples with cobalt-zinc ferrite. The attenuation coefficient can be counted from dissipation, neglecting the effect of multiple wave interference in the sample. The results for several samples of nanocomposites with particles of nickel-zinc ferrite are presented in Fig. 5b. The samples have been subjected to annealing at different temperatures: 750, 1100, and 1200 °C. The largest attenuation coefficient is found in the sample with annealing at 750 °C. If samples are annealed at 1100 and 1200 °C, disrupting the periodic structure of the opal matrix, there is a partial dispersion of particles of ferrite, which leads to less dissipation.

Figure 6 summarizes the measuring results concerning the frequency dependences of transmission coefficients (a) and reflection coefficients (b) for the nanocomposites containing particles of ferrite spinels. In addition to the above written nanocomposites with particles of cobalt- and nickel-zinc ferrites, Fig. 6 shows other ones containing particles of manganese-zinc ferrite spinel. Comparison of the results shows that the transmission coefficient is the highest for the nanocomposites with particles of cobalt-zinc ferrite $Co_{0.35}Zn_{0.65}Fe_2O_4$. The lowest reflection coefficient is found for the nanocomposites with the particles of nickel-zinc ferrite, and the highest for the nanocomposites with the particles of manganese-zinc ferrite.

Let us see the results of the measurements of frequency dependences of transmission and reflection coefficients for the nanocomposites containing particles of cobalt ferrite spinel $CoFe_2O_4$, see Fig. 7. This ferrite does not contain zinc. Frequency changes for this nanocomposite are less pronounced than for the nanocomposite with particles of ferrite $Co_{0.35}Zn_{0.65}Fe_2O_4$. In Fig. 7, the approximation of experimentally measured dependences with calculated theoretically ones is shown. There is good agreement between the measured and calculated curves. The estimated values of complex permittivity are as follows: $\varepsilon' = 2.25$, $\varepsilon'' = 0.14$.

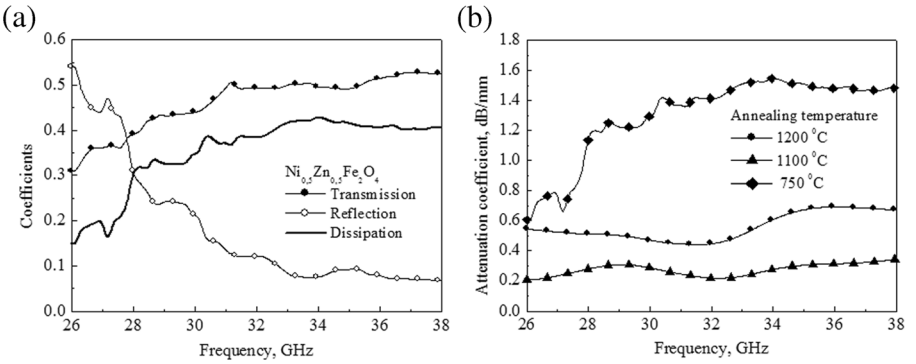

Fig. 5 The frequency dependences of the transmission and reflection coefficients and dissipation for the nanocomposites containing particles of nickel-zinc ferrite $Ni_{0.5}Zn_{0.5}Fe_2O_4$ (**a**); the frequency dependences of attenuation coefficients of electromagnetic waves in the nanocomposites with the particles of nickel-zinc ferrite $Ni_{0.5}Zn_{0.5}Fe_2O_4$, annealed at different temperatures (**b**)

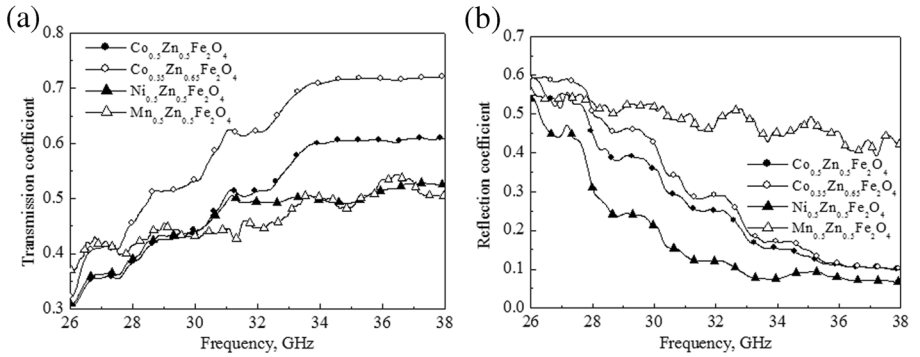

Fig. 6 The frequency dependences of transmission coefficients (**a**) and reflection coefficients (**b**) for nanocomposites containing particles of ferrite spinels

3.3 Chromium Spinels

Let us consider the dielectric properties of chromium spinels. Figure 8 shows the frequency dependences of transmission and reflection coefficients, and dissipation power, for nanocomposite No. 303/5-900 containing particles of a nickel-chrome spinel $NiCr_2O_4$. Figure 8a shows the experimentally measured dependences and Fig. 8b the approximation with the calculated dependences. The tendency of increasing the transmission coefficient and reducing the reflection coefficient with increasing frequency is also valid for this nanocomposite. Figure 8b shows that the approximation is performed quite well over a frequency range from 26 to 38 GHz, which confirms the weak frequency dispersion of dielectric permittivity of this nanocomposite in the selected frequency range. Permittivity values have been found as follows: $\varepsilon' = 2.62,\ \varepsilon'' = 0.04$.

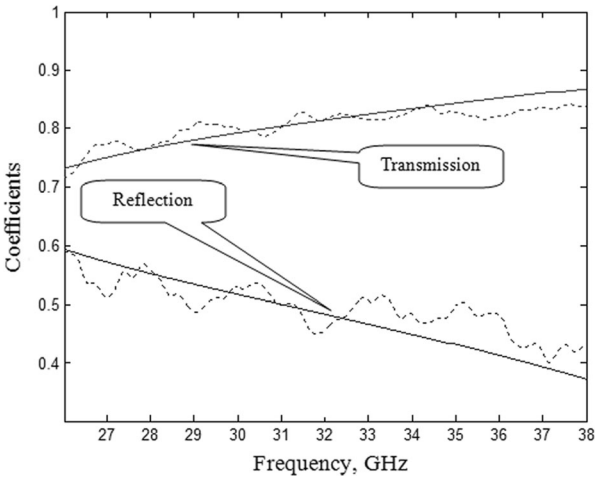

Fig. 7 The frequency dependences of the transmission and reflection coefficients along with their approximation by the calculated dependences for the nanocomposites containing particles of cobalt ferrite spinel $CoFe_2O_4$

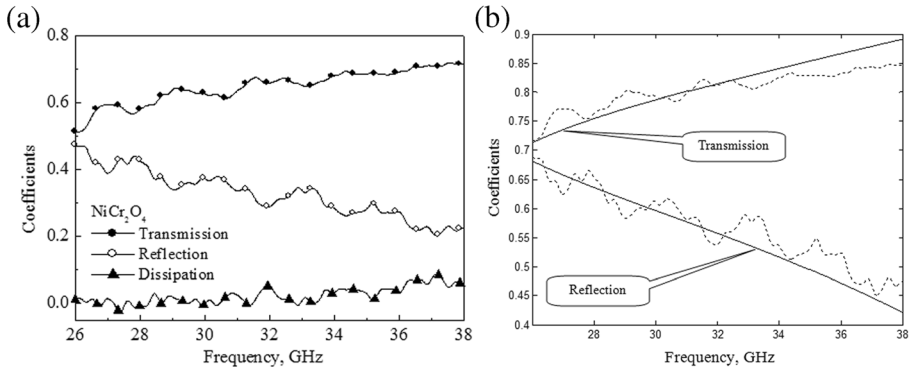

Fig. 8 The frequency dependences of transmission and reflection coefficients and dissipation for nanocomposite No. 303/5-900 containing particles of nickel-chrome spinel $NiCr_2O_4$: experimentally measured (**a**); approximation with the calculated dependences (**b**)

3.4 Manganese Spinels

Now we consider the high-frequency dielectric properties of nanocomposites with particles of manganese spinels. They typically have a chemical composition $MeMn_2O_4$, where Me is the transition metal of Fe or Ni.

In Fig. 9, the frequency dependences of transmission and reflection coefficients and dissipation for nanocomposites containing particles of manganese spinels are shown: (a) sample No. 210/5-900 with $FeMn_2O_4$ particles and (b) sample No. 211/5-900 with $NiMn_2O_4$ particles. The values of dielectric permittivity of these samples are given in Table. 2.

In this section, we have examined dielectric properties of the nanocomposites with the particles of the spinel formed by the metals Fe and Ni from period 3 and group VIII of the periodic system of elements. Next, we shall consider the properties of the nanocomposites with particles of spinel formed by titanium metal from the same period 3 and group IV of the periodic system. The frequency dependences of transmission and reflection coefficients and dissipation for nanocomposite No. 188/6-900, containing particles of titanium-manganese spinel $TiMn_2O_4$, are shown in Fig. 10, and the numerical values of its complex permittivity are given in Table. 2. The real part of permittivity of this nanocomposite is the highest among all the studied manganese spinels.

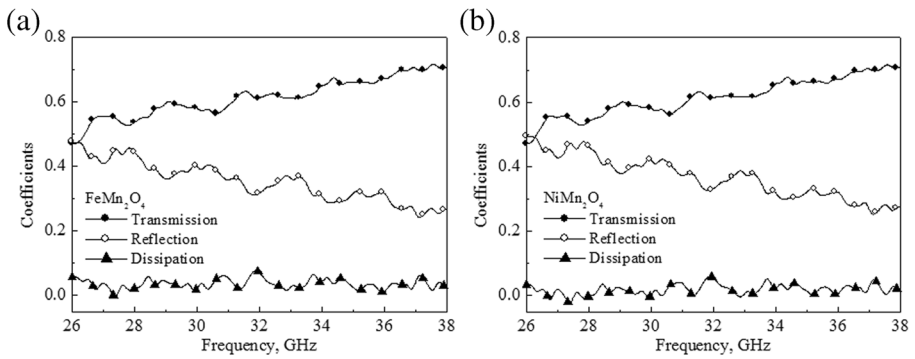

Fig. 9 The frequency dependences of transmission and reflection coefficients and dissipation for nanocomposites containing particles of manganese spinels: sample No. 210/5-900 with $FeMn_2O_4$ particles (**a**); sample No. 211/5-900 with $NiMn_2O_4$ particles (**b**)

Table 2 The complex dielectric permittivity of composites with spinel nanoparticles estimated in the frequency range from 26 to 38 GHz

Sample's name	The composition of the sample	ε'	ε''
No 2/0-900	Opal matrix (empty)	2.51	0.12
No 20/8-900	Opal matrix + $Co_{0.35}Zn_{0.65}Fe_2O_4$	3.90	0.19
No 23/8-900	Opal matrix + $Co_{0.5}Zn_{0.5}Fe_2O_4$	3.90	0.47
No 15/9-900	Opal matrix + $Mn_{0.5}Zn_{0.5}Fe_2O_4$	4.81	0.41
No 13/12-900	Opal matrix + $Ni_{0.5}Zn_{0.5}Fe_2O_4$	5.53	0.84
No 488/5-810	Opal matrix + $Ni_{0.5}Zn_{0.5}Fe_2O_4$+ Pd	2.50	0.08
No 21/8-900	Opal matrix + $Mn_{0.34}Co_{0.34}Zn_{0.33}Fe_2O_4$	4.61	0.33
No 22/8-1000	Opal matrix + $La_{0.34}Co_{0.34}Zn_{0.33}Fe_2O_4$	4.23	0.26
No 141/7-900	Opal matrix + $Nd_{0.34}Co_{0.34}Zn_{0.33}Fe_2O_4$	3.30	0.25
No 223/5-900	Opal matrix + $CoFe_2O_4$	2.25	0.14
No 302/5-900	Opal matrix + $CoCu_2O_4$	2.41	0.11
No 305/5-900	Opal matrix + $CoCu_2O_4$	2.97	0.29
No 303/5-900	Opal matrix + $NiCr_2O_4$	2.62	0.04
No 309/5-900	Opal matrix + $NiCr_2O_4$	2.58	0.06
No 210/5-900	Opal matrix + $FeMn_2O_4$	2.69	0.07
No 211/5-900	Opal matrix + $NiMn_2O_4$	2.72	0.04
No 226/5-900	Opal matrix + $CoMn_2O_4$	2.25	0.06
No 209/4-900	Opal matrix + $CoMn_2O_4$	2.75	0.13
No 188/6-900	Opal matrix + $TiMn_2O_4$	2.99	0.03

3.5 Copper Spinels

Among the nanocomposites containing particles of copper spinels, that are the substances with the chemical formula $MeCu_2O_4$, we consider the nanocomposites with the particles of cobalt-copper spinel. The frequency dependences of transmission and reflection coefficients and dissipation for nanocomposite No. 305/5-900, containing particles of cobalt-copper spinel $CoCu_2O_4$, are shown in Fig. 11. Figure 11a shows the experimentally measured dependences,

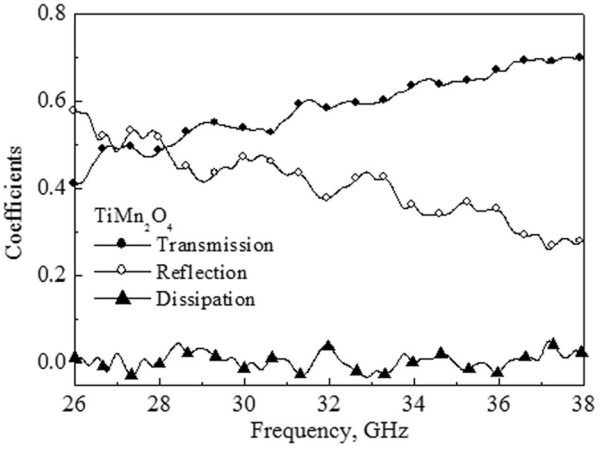

Fig. 10 The frequency dependences of transmission and reflection coefficients and dissipation for nanocomposite No. 188/6-900 containing particles of titanium-manganese spinel $TiMn_2O_4$

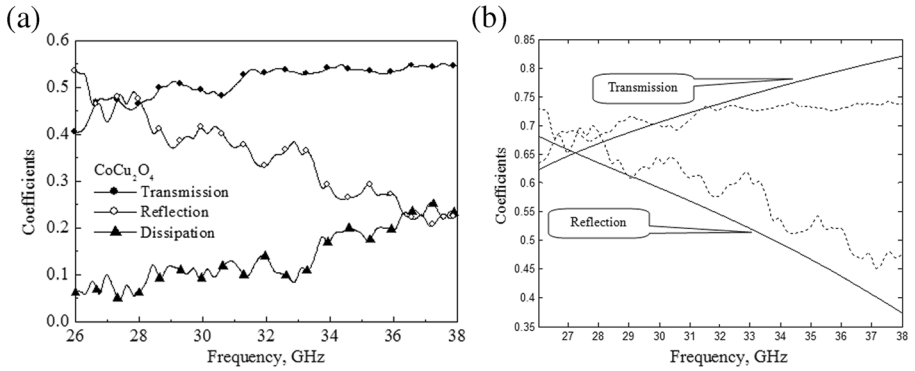

Fig. 11 The frequency dependences of transmission and reflection coefficients and dissipation for nanocomposite No. 305/5-900 containing particles of cobalt-copper spinel $CoCu_2O_4$: experimentally measured (**a**); approximation with the calculated dependences (**b**)

and Fig. 11b displays their approximation with the calculated dependences. From the approximation, the estimated values of complex permittivity of the nanocomposite have been obtained: $\varepsilon' = 2.97$, $\varepsilon'' = 0.30$.

It should be noted that the approximation made for the same value of dielectric permittivity within the whole frequency range does not provide a complete coincidence of experimental and calculated curves. It is possible that this discrepancy is a consequence of frequency dispersion of dielectric permittivity for this nanocomposite.

4 Models of Effective Permittivity

In this article, the nanocomposites based on opal matrix and containing particles of different spinels in interspherical volumes are under discussion. To obtain such nanocomposite materials with desired permittivity, it is important to explore the possibility of describing their properties using an effective permittivity. Next, you need to figure out which of the known variants of introduction of an effective permittivity is better suited to describe properties of materials of the type under consideration. First, we calculate the effective dielectric permittivity for an empty opal matrix considering it as a composite material. We assume that the nanospheres of SiO_2 with the dielectric permittivity $\varepsilon_m = 3.7$ form the matrix in the model of effective medium. The volume fraction of nanospheres in the opal is $v_m = 0.75$. The interspherical voids have the dielectric permittivity $\varepsilon_f = 1$. Let us perform calculations for effective permittivity using three options for introducing an effective environment, as it has been done in the article [12]. First, we calculate the effective permittivity according to the formula proposed in [13]:

$$\varepsilon_{eff} = \frac{\varepsilon_m(1-v_f) + \varepsilon_f v_f \left[\frac{3\varepsilon_m}{\varepsilon_f + 2\varepsilon_m}\right] \cdot \left[1 + \left(\frac{3v_f(\varepsilon_f - \varepsilon_m)}{\varepsilon_f + 2\varepsilon_m}\right)\right]}{1 - v_f + v_f \left[\frac{3\varepsilon_m}{\varepsilon_f + 2\varepsilon_m}\right] \cdot \left[1 + \left(\frac{3v_f(\varepsilon_f - \varepsilon_m)}{\varepsilon_f + 2\varepsilon_m}\right)\right]} \tag{10}$$

Substituting the numerical values for empty opal matrix, we obtain that $\varepsilon_{eff} = 3.52$.

Now we perform a similar calculation using the formula proposed in [14]:

$$\ln\varepsilon_{eff} = \left(1-\upsilon_f\right)\ln\varepsilon_m + \upsilon_f \ln\varepsilon_f \tag{11}$$

For empty opal matrix, we get here the value $\varepsilon_{eff} = 2.71$.

Then perform the calculation according to the effective medium theory EMT [15]. The equation has the form

$$\varepsilon_{eff} = \varepsilon_m\left[1 + \frac{\upsilon_f\left(\varepsilon_f-\varepsilon_m\right)}{\varepsilon_m + n\left(1-\upsilon_f\right)\left(\varepsilon_f-\varepsilon_m\right)}\right], \tag{12}$$

where n is the corrective factor depending on the shape of the filler. At first we take $n = 0.15$ by analogy with [12]. The calculation results in $\varepsilon_{eff} = 3.02$. According to our measurements over a frequency range 26–38 GHz, the complex dielectric permittivity of empty opal matrix is $2.51 + i{\cdot}0.12$. Comparing it with the results, we have calculated using the formulas (9, 10, 11); one can see that acceptable results are obtained by introducing an effective permittivity on the second and third embodiments, and the formula (10) proposed in [13] gives an inflated result. Selection of the values of corrective factor for the experimental value of $\varepsilon_{eff} = 2.51$ leads to the choice $n = 0.81$, more appropriate for our materials. Below we use this value n to estimate the dielectric permittivity of the nanocomposites with the particles of $NiCr_2O_4$. Taking $\varepsilon_m' = 2.5$ for opal matrix and $\varepsilon_f = 11.8$ for particles of the nickel-chrome spinel [16] and $v_f = 0.09$, we get from formula (12) that $\varepsilon_{eff} = 2.58$, which is close to the measured values $\varepsilon_{eff} = 2.62$ and $\varepsilon_{eff} = 2.58$, see Table 2.

The values of dielectric permittivity of the nanocomposites presented in Table 2, essentially vary from those taken from literature for the corresponding bulk materials. This is not surprising because spinel particles occupy only a little part of the whole volume of the nanocomposites. As a rule, the real part of dielectric permittivity of nanocomposites falls into the interval between the empty opal matrix and the bulk material of particles. For example, for the nanocomposites with $CoFe_2O_4$ particles, the value $\varepsilon_{eff}' = 2.25$ is given in Table 2, whereas for bulk $CoFe_2O_4$ $\varepsilon' = 10$ at frequency $f = 4.55$ GHz [17], and also can be equal from 3 to 5 depending of the annealing temperature [18]. The presence of residual water, besides the material of particles, can substantially influence the imaginary part of permittivity. It is known from literature that dielectric permittivity is strongly dependent on frequency and temperature. Partially, for nickel-zinc ferrite spinel, $Ni_{0.5}Zn_{0.5}Fe_2O_4$ dielectric permittivity equals $\varepsilon' = 132$ at frequency 1 MHz [18]. In the work in [19] for nickel ferrite, $\varepsilon' = 12.7$ at 12 GHz is obtained. So, the value $\varepsilon' = 5.53$ obtained in our work for the nanocomposites with $Ni_{0.5}Zn_{0.5}Fe_2O_4$ particles looks reasonable.

From Table 2, it follows that the largest value of the real part of dielectric permittivity ε' has the next samples: No. 13/12-900 with particles of $Ni_{0.5}Zn_{0.5}Fe_2O_4$, No. 15/9-900 with particles of $Mn_{0.5}Zn_{0.5}Fe_2O_4$, and No. 21/8-900 with particles of $Mn_{0.34}Co_{0.34}Zn_{0.33}Fe_2O_4$. Of course, the value of dielectric permeability of nanocomposites depends not only on dielectric permittivity of the introduced substance but also on the volume fraction of the impregnated substance. Minimal values of the real part of dielectric permittivity have samples No. 223/5-900 with particles of $CoFe_2O_4$ and No. 226/5-900 with particles $CoMn_2O_4$. Also it is seen that the largest values of ε'' have the following specimens: No. 13/12-900 with particles of $Ni_{0.5}Zn_{0.5}Fe_2O_4$, No. 23/8-900 with $Co_{0.5}Zn_{0.5}Fe_2O_4$ particles, and No. 15/9-900 with particles of $Mn_{0.5}Zn_{0.5}Fe_2O_4$. As we can see, the highest values for both the real and imaginary parts of dielectric permittivity belong to the ferrite spinels. The lowest values ε'' correspond to

the samples No. 188/6-900 with particles of $TiMn_2O_4$, No. 303/5-900 with particles of $NiCr_2O_4$, and No. 211/5-900 with $NiMn_2O_4$ particles.

5 Conclusion

We have studied high-frequency dielectric properties of 3D nanocomposite materials based on opal matrix, the interspherical cavities in which are partially filled with the particles of spinels of several types. Among the investigated fillers are the ferrite spinel composition $Me1_xMe2_{1-x}Fe_2O_4$, where Me1 is a transition metal of Fe or Ni, Me2 is zinc, the chrome spinel composition $MeCr_2O_4$, the manganese spinels $MeMn_2O_4$, the copper spinels $MeCu_2O_4$, and some other materials with spinel structure. Measurement of dielectric properties has been made using the waves of millimeter waveband at frequencies from 26 to 38 GHz. The measured frequency dependences of reflection and transmission coefficients have been obtained with the use of nanocomposite samples with the thickness of 2 mm. From the received dependences, we determined the real and imaginary parts of complex permittivity of the nanocomposites. A comparison of the experimental and calculated frequency dependences is performed. The main conclusion that can be drawn from the carried out research is that choosing the chemical composition and temperature of the thermal treatment of nanocomposites makes it possible to produce the dielectric materials with the desired value of real part of high-frequency dielectric permittivity varying between 2.3 and 5.5. The nanocomposites having a minimal imaginary part of the dielectric permittivity can be used for elements of microwave devices where it is necessary to ensure low absorption of microwaves. The nanocomposites with the particles of ferrite spinels $Ni_{0.5}Zn_{0.5}Fe_2O_4$, $Co_{0.5}Zn_{0.5}Fe_2O_4$, and $Mn_{0.5}Zn_{0.5}Fe_2O_4$ having maximal imaginary parts of permittivity can be used as absorbers of millimeter waves.

Acknowledgments The X-ray phase analysis of the nanocomposites and investigation of their structure are performed in the Collaborative Access Center of Institute of Metal Physics. This work is carried out within the theme “Spin” No. 01.2.006 01201463330, with partial support of grant from Russian Ministry of Education and Science No.14.Z50.31.0025 and grant No. 15-9-2-12.

References

1. Photonic glasses, F. Gan, L. Xu, Eds. (New Jersey, London: World Scientific Press, 2006).
2. A.K. Sarychev, V.M. Shalaev, Electrodynamics of metamaterials (New Jersey, London: World Scientific Press, 2007).
3. S.O. Demokritov, A.N. Slavin, Magnonics: from fundamentals to applications (Berlin, Heidelberg: Springer, 2012).
4. A.B. Rinkevich, A.M. Burkhanov, M.I. Samoilovich, A.F. Belyanin, S.M. Klescheva, E.A. Kuznetsov, Rus. J. Gen. Chem., 83(11), 2148–2158 (2013).
5. V.V. Ustinov, A.B. Rinkevich, D.V. Perov, M.I. Samoilovich, S.M. Klescheva, JMMM, 324(1), 78–82 (2012).
6. V.V. Ustinov, A.B. Rinkevich, D.V. Perov, A.M. Burkhanov, M.I. Samoilovich, S.M. Klescheva, E.A. Kuznetsov, Tech. Phys., 58, 568–577 (2013).
7. A.B. Rinkevich, E.A. Kuznetsov, D.V. Perov, Yu.I. Ryabkov, M.I. Samoylovich, S.M. Klescheva, Int. J. Infrared Milli. Terahz. Waves, 35(10), 860–870 (2014).
8. A.B. Rinkevich, A.M. Burkhanov, D.V. Perov, M.I. Samoilovich, S.M. Kleshcheva, E.A. Kuznetsov, Photonics Nanostruct., 12, 144–151 (2014).

9. A.B. Rinkevich, L.N. Romashev, V.V. Ustinov, E.A. Kuznetsov, Int. J. Infrared Milli. Waves, 28, 567–578 (2007).
10. A.B. Rinkevich, M.I. Samoilovich, S.M. Klescheva, D.V. Perov, A.M. Burkhanov, E.A. Kuznetsov, IEEE Trans. Nanotechnol., 13(1), 3–9 (2014).
11. M. Pardavi-Horvath, JMMM, 215–216, 171–183 (2000).
12. T.S. Sasikala, M.T. Sebastian, J. Electr. Mater., 45(1), 729–735 (2016).
13. N. Jayasundere, B.V. Smith, J. Appl. Phys., 73, 2462 (1993).
14. K. Wakino, T. Okada, N. Yoshida, K. Tomono. J. Am. Ceram. Soc., 76, 2588 (1993).
15. Y. Rao, J.M. Qu, T. Marinis, C.P. Wong, IEEE Trans. Compon. Packag. Technol., 23, 680 (2000).
16. N. Mufti, A.A. Nugroho, G.R. Blake, T.T.M. Palstra, J. Phys. Condens. Matter, 22, 075902 (2010).
17. T. Okamura, T. Fujimura, M. Date Phys. Rev., v.85, p.1041-1042 (1952)
18. R.C. Kambale et al. Journal of Alloys and Compounds, 491, 372–377 (2010)
19. I. Tsiachristos et al. EPJ Web of Conferences 75, 06005 (2014)